Mixing sensitivity to the inclination of the lateral walls in a T-mixer

A. Mariotti[a], C. Galletti[a,*], E. Brunazzi[a,*], M.V. Salvetti[a]

[a] *Dipartimento di Ingegneria Civile e Industriale, Università di Pisa, Largo Lazzarino, 2, 56122 Pisa, Italia*

Abstract

One of the simplest geometries for micro-mixers has a T-shape, i.e., the two inlets join perpendicularly the mixing channel. The cross-sections of the channels are usually square/rectangular, as straight walls facilitate experimental and modeling analysis. On the contrary, this work investigates through Computational Fluid Dynamics the effect of a cross-section with lateral walls inclined of an angle α as such an inclination may stem from different microfabrication techniques. Considering water as operating fluid, the same mixing performance as square/rectangular cross-sections is obtained for inclinations $\alpha \leq 3°$; this indicates the maximum admissible error on the perpendicularity of the walls in the manufacturing process. Above this value, the presence of inclined walls delays the onset of the engulfment regime at higher Reynolds numbers, and for $\alpha \geq 23°$ the mixing is hampered dramatically, as the flow is unable to break the mirror symmetry and enter in the engulfment regime. At low Reynolds numbers, the mixing is moderately improved for $\alpha \geq 10°$,

*Corresponding author

Email addresses: alessandro.mariotti@for.unipi.it (A. Mariotti), chiara.galletti@unipi.it (C. Galletti), elisabetta.brunazzi@unipi.it (E. Brunazzi), mv.salvetti@ing.unipi.it (M.V. Salvetti)

because the vortex regime presents a lower degree of symmetry than that of T-mixers with straight walls.
Keywords: T-shaped micro-mixer, lateral-wall inclination, trapezoidal cross-section, flow regimes, mixing degree

1. Introduction

Microfluidic devices consist of a pattern of microchannels, molded or engraved, with typical dimensions < 1 mm. The interest towards them is motivated by the unique features that miniaturization provides, viz. huge surface-to-volume ratio strongly improving the heat transfer, small volume of samples and fast response time. These characteristics, for instance, offer the chance to handle highly exothermic or dangerous reactions without the need for dilution. Indeed, microfluidics is appealing for intensifying processes in the pharmaceutical [1] or fine chemicals fields, by allowing the setup of greener and more sustainable chemical routes with less consumption of reactants and energy and less waste [2–5].

However, the use of microfluidic devices for process intensification has to face a major challenge related to the efficient mixing of reactants. Indeed, the flow is laminar and mixing occurs solely through diffusion unless mixing enhancement techniques are adopted. Among them, passive methods are preferred as they do not need any external energy source, rather promoting mixing through a special arrangement of the inlet and mixing channels aimed at triggering convection [6].

Although significant advancements have been made on both additive and subtractive microfabrication technologies, which nowadays allow complex

3-dimensional geometries to be generated, simple microdevice geometries are desirable. Examples of widely employed and simple designs are T-, arrow- [7], Y- and cross-shaped [8, 9] ones. The cross-section geometry of the channel is usually square or rectangular [10–12], only in a few cases circular [13]. Despite the very basic geometry and the laminar regime, the fluid dynamics, which determines the mixing process, is very complex. Indeed, different steady regimes have been identified for the above micromixer geometries depending on the Reynolds number, i.e, Re [14–16]. Moreover, some time-periodic unsteady motions were observed to be triggered in specific conditions still in the laminar regime, i.e., see [17–20] for the T-shaped mixer; [21] for the arrow-shaped mixer and [8] for the cross-mixer.

In T-shaped micromixers, at low Re the fluid streams entering the microdevice remain segregated in the mixing channel, flowing side by side, with a little degree of mixing due to diffusion. As we augment the flow rates, a recirculation region forms at the top of the mixer and generates two U-shaped vortical structures, whose legs extend in the mixing channel. Such a regime presents a high level of symmetry, and thus mixing is poor. With further increasing the Reynolds number, the top part of the U-shaped structures tilts and subsequently one leg of each vortical structure becomes stronger than the other [22]. This behavior stimulates a symmetry breaking, triggering the so-called engulfment regime, with a sudden increase of the degree of mixing. Then, the flow becomes unsteady and periodic; the features of different periodic regimes can be found, e.g., in [17, 23]. A recent review on the flow regimes occurring in a T-shaped micromixer has been provided by Camarri et al. [11], while extensive literature is available on the effect of fluid properties

[24, 25], channel aspect ratio [26, 27] on the flow regimes and mixing. The role of flow features and chemical kinetics on the reaction yield have been recently investigated in [28, 29].

However, all the above investigations refer to microdevice with cross sections having perfectly perpendicular walls. Therefore, possible inaccuracies of the cross-section geometry related to the micro-fabrication technology, are not taken into account. In fact, some techniques may generate lateral walls of the micro-channels that are not perfectly perpendicular to the bottom plane. This feature for instance occurs in the case of channels that are engraved through chemical etching. Indeed, micro-mixers with trapezoidal cross-sections may be fabricated more easily than those with square/rectangular cross-sections by using anisotropic KOH etching of silicon [30]. Recently Lee et al. [31] showed how different microchannel cross-sections could be realized by using anisotropic wet etching of Si wafer and self-alignment between Si structure and PDMS mold. Peng et al. [32] suggested a low-cost strategy for the fabrication of micro-channels on silicon substrate based on direct marker pen ink writing and metal-assisted chemical etching, showing how the composition of the etchant solution has a great influence on the resulting 3D profiles of the microchannels, which exhibit trapezoidal cross-sections [32]. Also, other microfabrication techniques such as those based on laser ablation can lead to microchannels with trapezoidal cross-sections, as in the case of CO_2 laser with a polymethilmetacrilate (PMMA) substrate [33–35] or of a femtosecond laser to engrave glass wafers [36].

In our recent paper [35], we investigated the mixing process in a T-shaped mixer exhibiting a trapezoidal cross section with the lateral walls inclined by

$\alpha = 25°$ to the vertical plane. Such geometry resembles the one that can be obtained with laser on PMMA. This fabrication procedure involves the cutting of a PMMA layer with a laser beam and subsequently the bonding of this layer within two additional layers in a sandwich-like manner. More details on fabrication are given in [35], which also reports typical values of characteristic width and depth of the cut region as a function of the laser energy density. We observed that this configuration hampers the bifurcation triggering the engulfment regime, which hence occurs at a larger Reynolds number with respect to the corresponding T-mixer with vertical sidewalls. However, at low Reynolds the mixing is enhanced because the vortical structures in the mixing channels have different strengths as a consequence of the trapezoidal shape of the cross section and this helps mixing.

This background motivates the present work, which is aimed at carrying out a comprehensive investigation of the effect of lateral-wall inclination on flow regimes occurring in a T-shaped micro-mixer and hence on the mixing process. For this purpose, numerical simulations are carried out for different values of the inclination angle in the range $0 \leq \alpha \leq 25°$, with $\alpha = 0$ corresponding to the mixer with square/rectangular cross sections. The maximum value of the inclination angle ($\alpha = 25°$) was selected according to classical values of wall inclination obtained with laser cutting on PMMA. Since most studies in the literature have been carried out for $\alpha = 0°$, we decided to investigate the whole range of variation of wall-inclination angles from $\alpha = 0°$ to $\alpha = 25°$ to cover all typical α values that may be encountered with different microfabrication techniques.

The goal is to provide practical information on how the uncertainty on

sidewall inclination stemming from microfabrication affects the flow regimes and mixing by providing, e.g., quantitative relationships between the lateral-wall inclination, the critical Reynolds numbers of different flow regimes and the related mixing degree. Indeed, the fluid dynamics of microchannels with trapezoidal cross-sections has been poorly investigated in literature. The study in [36] proposes trapezoidal cross-sectional spiral channels to generate stronger Dean drag force for the separation of microparticles and cells. Therefore, trapezoidal cross sections might be interesting from a practical viewpoint for some applications. The present study can thus help also in highlighting whether this geometry may have potential positive features.

2. T-mixer geometry and operating conditions

The investigated mixer has a T-shape with a trapezoidal cross-section. It is sketched in Fig. 1 together with the reference system. The mixer has the same inclination, α, of the inlet and mixing channel lateral walls. Fourteen different values of α are considered within the range of variation of $1.8° - 25°$. The mixing channel cross-section area is double the inlet ones (the two inlet channels are identical) to have no acceleration effects, i.e. the mean fluid velocity in the two inlets, U, is the same as the mean fluid velocity in the outlet. The height of the channels is $h = 1$ mm, the top and bottom widths of the inlet channels are b_i and w_i, with $b_i > w_i$ and $(b_i + w_i) = 2h$, whereas the top and bottom widths of the mixing channel are b_o and w_o, with $b_o > w_o$ and $(b_o + w_o) = 4h$. Consequently, the hydraulic diameter of the inlet channels, $d_i = \frac{2h}{1+1/cos(\alpha)}$, ranges from $d_i = 1$ mm to $d_i = 0.95$ mm with α, whereas the hydraulic diameter of the mixing channel, $d = \frac{4h}{2+1/cos(\alpha)}$, ranges from $d = 1.33$

mm to $d = 1.29$ mm. The length of the inlet channels is $l_i = 20d$ to allow the flow to be fully developed at the confluence of the two inlet streams, while the length of the mixing channel is $l_o = 30d$. In the following, all uppercase coordinates are made non-dimensional by using the hydraulic diameter of the mixing channel, d, e.g. $X = x/d$, $Y = y/d$ and $Z = z/d$.

The T-mixer is fed with water at ambient conditions and equal flow rates from the two inlets. Simulations have been carried out for Reynolds numbers in the range $Re = \frac{Ud}{\nu} = 50 \div 350$, with ν being the kinematic viscosity of the fluid.

3. Numerical methodology and simulation set-up

The fluid motion is completely described through the Navier-Stokes equations. The non-dimensional form of the equations for an incompressible fluid is:

$$\nabla \cdot \mathbf{u} = 0 \tag{1}$$

$$\frac{\partial \mathbf{u}}{\partial \theta} + \mathbf{u} \cdot \nabla \mathbf{u} = -\nabla P + \frac{1}{Re} \nabla^2 \mathbf{u} \tag{2}$$

where $\partial/\partial\theta$ is the time derivative and P is the modified non-dimensional pressure. The time is normalized using the convective time d/U, the lengths using the hydraulic diameter d of the mixing channel, while the velocities $\mathbf{u}$ through the bulk velocity U.

The above equations are coupled with a transport equation for the dye mass fraction ϕ to distinguish between the two inlet water streams:

$$\frac{\partial \phi}{\partial \theta} + \mathbf{u} \cdot \nabla \phi = \frac{1}{Pe} \nabla^2 \phi, \tag{3}$$

where $Pe = Ud/D$ is the Peclet number, with D being the molecular diffusivity of the dye. Since for liquids the Schmidt number is very large, i.e. $Sc = \mu/(\rho D) = O(10^3 - 10^4)$, the resulting Peclet number is $Pe = Sc \cdot Re = O(10^6)$ ([23]).

The steady-state solver of the finite volume code ANSYS Fluent v.19 is employed to solve the above equations. A second order upwind interpolation scheme is used for spatial discretization. The SIMPLE algorithm is adopted to treat the pressure-velocity coupling.

The computational grid is fully structured with 4.7 M cells; the trapezoidal cells are equally long in all directions at the confluence region, while they elongate along the inlet and the outlet channels. In a cross-section of the mixing channel, there are 40×80 cells. The computational grid in the limit case of perpendicular walls, i.e. for $\alpha = 0°$, has been widely validated in our previous studies (see e.g. [16, 23]). Such a fine grid has a number of cells well above the minimum one suggested in [37], i.e. 20 cells within the shortest characteristic length. In the above our papers, we also showed that the grid was able to capture the concentration field. Since $Sc \gg 1$, a rigorous simulation of the dye distribution would require a grid much finer than that suited for the flow field; this implies that mass diffusion is estimated on a coarse-grained size [38]. This affects results for small Re, at which diffusion dominates the mixing process with a typical length of about $d/\sqrt{Pe}$. However, in the present paper, we focus on much higher Re numbers for which convection at the confluence occurs also along a transverse direction, i.e., perpendicularly to the mean flow, implicating that each fluid stream penetrates into the other by much larger distances. Further discussion on

this issue can be found in Galletti et al [39].

The same fully structured grid is stretched for the simulations with inclined walls. Cubic cells become trapezoidal cells with an inclination of the lateral sides equal to α. Grid independence has been checked for the simulation in the maximum wall inclination, i.e. in the case with $\alpha = 25°$, at $Re = 350$. Differences between the results obtained for the grid with 4.7 M cells and for a finer one with 7.35 M cells are below 0.15% in terms of the mixing degree estimated at the $Y = -25$ cross section. In this section, the averaged difference between the two grids in terms of the velocity field, evaluated by using the L2 norm, is below 0.25%.

Such numerical setup has been also successfully benchmarked against a massive parallel spectral element code in [23], and validated against experimental flow visualizations for a T-mixer with perpendicular walls in [16].

4. Results

The mixing performance of the T-mixer having different trapezoidal cross-sections is quantified by using the mixing degree $\delta_m(Y)$, defined as in [21, 23], i.e.:

$$\delta_m(Y) = 1 - \frac{\sigma_b(Y)}{\sigma_{max}}, \tag{4}$$

where $\sigma_b(Y)$ is the standard deviation of the dye volumetric flow at the Y cross section and σ_{max} is the maximum value of σ_b, which is obtained for completely segregated streams. Thus, δ_m varies between $\delta_m = 0$, indicating a completely segregated flow, and $\delta_m = 1$, corresponding to a perfectly mixed flow.

The mixing degree at $Y = -8$ cross section, obtained for the different values of wall-inclination angles α is presented as a function of the Reynolds number in Fig. 2(a). A three-dimensional view of δ_m in the $\alpha - Re$ parameter space is shown in Fig. 2(b). The curves are interrupted at different Re for the various α, as our analysis is limited only to steady flow conditions and hence does not cover the unsteady motions that occur at higher Re. The results for the T-mixer with square inlet cross sections, i.e. $\alpha = 0°$ ([17]), is also reported here for comparison. It is clear that three different behaviors for the mixing degree with increasing Re can be observed for different inclination angles α: (i) for $\alpha \leq 8.7°$ an analogous behavior as for $\alpha = 0°$ occurs, i.e. for Reynolds numbers below a critical value $Re \leq Re_{cr,eng}$ ([16, 17]) the mixing degree is very low, then the δ_m undergoes a sudden increase, (ii) for $10° \leq \alpha \leq 22.6°$ a moderate increase in the mixing degree is found for $Re \leq Re_{cr,eng}$, above $Re_{cr,eng}$ a sudden increase of δ_m is again present, (iii) for $23° \leq \alpha \leq 25°$ moderate values of δ_m are present in the whole range of the investigated Reynolds numbers and a monotonic slightly increase in the mixing degree is found with increasing Re, without any sudden change.

The three-dimensional vortical structures in the T-mixer are presented in Figs. 3, 4 and 5 to describe the flow patterns occurring in the device for different values of α, viz. $\alpha = 1.8°$, $\alpha = 8.7°$, $\alpha = 18°$, and $\alpha = 25°$, and of Reynolds number, viz. $Re = 100$, $Re = 150$, and $Re = 200$. The vortical structures are identified through the λ_2 criterion ([40]), which defines a vortex as a connected fluid region where the second largest eigenvalue of the symmetric tensor $\mathbf{L} = \mathbf{S} \cdot \mathbf{S} + \mathbf{A} \cdot \mathbf{A}$ is negative. Here, $\mathbf{S}$ and $\mathbf{A}$ are the symmetric and anti-symmetric parts of the velocity gradient, i.e. the

strain rate and vorticity tensors, respectively. The dye-concentration, the in-plane velocity vectors and the normal-vorticity fields obtained at $Y = -8$ cross sections in the mixing channel are also shown in these figures to give a graphical explanation of the different behaviors of δ_m in Fig. 2.

First, we consider the results at $Re = 100$ that are shown in Fig. 3. From the dye concentration field, we can see that the flow is almost segregated for $\alpha = 1.8°$ and $\alpha = 8.7°$ with only diffusion at the vertical interface (Figs. 3(a,b)). On the contrary, the cases having $\alpha = 18°$ and $\alpha = 25°$ show a still segregated flow, albeit small regions of increased mixing can be observed in correspondence of the upper and lower walls (Figs. 3(c,d)), which lead to the moderate increase in δ_m shown in Fig. 2. In all cases, the 3D visualizations of the isocontours of the vortex-indicator λ_2 show the presence of two U-shaped vortical structures, whose top parts are located at the confluence of the two inlet streams, and stem from two flow recirculation regions formed near the top wall. The two legs of each U-shaped structures are counter-rotating and develop with almost equal strength in the mixing channel for $\alpha = 1.8°$ and $\alpha = 8.7°$ (Figs. 3(a,b)). The behavior resembles that of the *vortex regime* for $\alpha = 0°$ (presented in [16]), where the four legs have exactly equal strengths and the flow field, in that case, is characterized by perfect two-reflectional symmetries. As a result, for these values of α, at $Re = 100$ mixing occurs only by diffusion and, hence, remains very low. Instead, for $\alpha = 18°$ and $\alpha = 25°$ (Figs. 3(c,d)), we can see the strongest pair of legs moving towards the center of the section, and the weaker pair towards the lower wall, still preserving the mirror symmetry with respect to the channel mid-plane. Only the two strongest legs survive further down along the mixing channel, while

the weakest ones disappear because of the interaction of near-wall vorticity. Thus, also for the larger values of α at $Re = 100$ mixing is related mainly to diffusion but the somewhat greater intensity of the two counter-rotating stronger legs promotes a moderate increase in the degree of mixing by breaking one of the two reflectional symmetries.

Figure 4 shows the vortical structures, the dye distributions, and the corresponding vorticity fields at $Re = 150$. Again, four values of the lateral-wall inclination are considered. For $\alpha = 1.8°$ and $\alpha = 8.7°$, the $y-$vorticity fields at section $Y = -8$ (bottom-right panel in Fig. 4a,b) are characterized by two prevailing co-rotating vortices that enable mixing through convection and produce S-shaped flow patterns in cross sections of the mixing channel, with each inlet fluid stream being able to reach the opposite wall (top-right panel in Figs. 4a,b). This behavior is analogous to what happens in the *engulfment regime* of a T-mixer with $\alpha = 0°$ (see [16]). Differently from the latter case, here we also observe the formation of a weaker counter-rotating region between the two co-rotating vortices. The weaker counter-rotating region corresponds to the merging of the two weak legs, which progressively disappear along the mixing channel, as confirmed by the isocontours of the vortex indicator λ_2 (left and central panels of Figs. 4a,b). Moreover, the two stronger legs are different in strength with the co-rotating region for $Y < 0$ that is wider compared with the other, especially for $\alpha = 8.7°$. Conversely, Figs. 4c,d show again two stronger counter-rotating vortices at $Re = 150$ for $\alpha = 18°$ and $\alpha = 25°$. The mirror symmetry with respect to the channel mid-plane is not broken, and therefore the flow keeps remaining segregated, although presenting some moderate mixing. Therefore, for these largest angles

the flow is not entered yet in the engulfment regime at $Re = 150$.

At $Re = 200$ also the case $\alpha = 18°$ shows the engulfment regime (see Fig. 5c). The S-shape distribution of the dye on the cross-section at $Y = -8$ is indeed present for $\alpha = 1.8°$, $\alpha = 8.7°$ and $\alpha = 18°$ (top-right panels of Figs. 5a-c) and the corresponding $y-$vorticity fields exhibit the presence of the two co-rotating vortices (bottom-right panels of Figs. 5a-c). It should also be noted that for $\alpha = 1.8°$ and $\alpha = 8.7°$ the counter-rotating vortex between the two co-rotating vortices becomes weaker than for $Re = 150$, because the two weaker legs have already disappeared at the considered section (compare Figs. 4a,b at $Re = 150$ with Figs. 5a,b at $Re = 200$). For $\alpha = 18°$, in the central panel of Fig. 5c we can distinguish in the middle of the two stronger and co-rotating legs, one of the counter-rotating weak legs, positioned in line with the other two, while the second weak leg, much weaker, remains closer to the wall and has become much weaker than the other, once again due to the interaction with the wall. In addition to this, the two stronger legs are significantly different in strength with the co-rotating one for $Y < 0$ that is again wider than the other. On the contrary, for $\alpha = 25°$ the flow continues to remain segregated in the vortex regime (top-right panel of Fig. 5d). Indeed, the bottom-right panel of Fig. 5d shows a pair of strong counter-rotating vortices with two weaker counter-rotating vortices outside, all four aligned horizontally. These vortical structures, clearly visible through the vortex indicator λ_2, keep the mirror symmetry so that the mixing process is hampered. By further increasing the Reynolds, the flow becomes unsteady and time-periodic for $\alpha = 1.8°, 8.7°$ and $18°$ at $Re = Re_{cr,unst}$, whose values are discussed in the following. Conversely, for $\alpha = 25°$ the vortical

structures are unable to break the mirror symmetry in the range of Reynolds $Re = 50 - 350$, so the flow remains segregated at least for Re up to 350.

To better characterize the micromixers, the pressure drops, i.e. Δp, estimated for different wall inclination angles are reported in Fig. 6 as a function of the Reynolds number. More specifically, the pressure drops are evaluated between the inlets and the $Y = -8$ cross-section (i.e., the same section used for estimating the mixing degree) and made non-dimensional with the case having perpendicular walls ($\alpha = 0°$) at $Re = 50$, i.e. $\Delta p_0 = 48Pa$. As we can see in Fig. 6, just a slight increase of pressure drops with α may be noticed for a fixed Reynolds. On the other hand, the different flow regimes occurring in the T-mixer have a negligible effect on pressure drops.

After having described the flow regimes occurring in the T-mixer with inclined walls, we focus again on Fig. 2 to derive quantitative relationships between δ_m, α, Re, $Re_{cr,eng}$ and $Re_{cr,unst}$. Let us start from the onset of the engulfment regime. The relevant values of $Re_{cr,eng}$ are reported as a function of α in Fig. 7(a), together with the corresponding degree of mixing at $Re = Re_{cr,eng}$ in Fig. 7(b). The critical value of the Reynolds number for $\alpha = 0°$ was found in [17] equal to $Re_{cr,eng}^{\alpha=0°} = 140$. The critical Re value for the engulfment onset remains the same as for $\alpha = 0$ for the two smaller considered inclination angles, i.e $\alpha = 1.8°$ and $\alpha = 3°$, whereas $Re_{cr,eng}$ slightly increases for $\alpha = 6°$ and $\alpha = 8.7°$, up to $Re_{cr,eng} = 146$ for $\alpha = 8.7°$. Despite this slight difference, the behavior of the mixing degree for $\alpha \leq 8.7°$ is analogous to that of $\alpha = 0°$, starting with an initial very low value of $\delta_m^{cr,eng}$ (see Fig. 7b) and then growing abruptly beyond $Re_{cr,eng}$. The trend after the engulfment onset looks similar and slightly shifted to larger values of Reynolds as the

angle of inclination increases. A monotone and more significant increase of $Re_{cr,eng}$ is found for $10° \leq \alpha \leq 22.6°$, reaching the maximum value of $Re_{cr,eng} = 185$ for $\alpha = 22.6°$. It should be noted also that in these cases the engulfment onset follows a regime of moderate mixing, thus the value of mixing at the onset of the engulfment regime, $\delta_m^{cr,eng}$, is more than 5 times higher than the one for $\alpha \leq 8.7°$ (see Fig. 7b). Nevertheless, the mixing degree for $Re \geq Re_{cr,eng}$ is analogous, even if shifted to higher Reynolds numbers, to those with lower values of the wall inclination (see Fig. 2). On the contrary, no values of $Re_{cr,eng}$ are found for $\alpha \geq 23°$, with the mixing degree that moderately increases with Reynolds, but remains considerably smaller than the one achieved with the other cases for $Re \geq Re_{cr,eng}$. Up to $\alpha = 23°$, all couples of engulfment onset values (α,$Re_{cr,eng}$) are nicely fitted by a square function as follows:

$$Re_{cr,eng} = 0.090\alpha^2 - 0.118\alpha + Re_{cr,eng}^{\alpha=0°}; \tag{5}$$

As for the Reynolds number at which the flow becomes unsteady, $Re_{cr,unst}$, [16] found $Re_{cr,unst}^{\alpha=0°} = 230$ for perfect perpendicular walls. The relevant results with wall inclinations are presented in Fig. 8a, together with the corresponding degree of mixing at $Re = Re_{cr,unst}$ in Fig. 8b. The same value of $Re_{cr,unst}$ as for $\alpha = 0°$ holds for $\alpha = 1.8°$ and $\alpha = 3°$. Since also the same value of $Re_{cr,eng}$ is found for $\alpha \leq 3°$, $\alpha = 3°$ can be considered the maximum admissible error in the manufacturing process on the perpendicularity of the walls of T-mixers operating with water-water to obtain the same performance as the nominal T-mixer configuration. For $\alpha > 3°$ the value of $Re_{cr,unst}$ monotonically increases (Fig. 8a), reaching the maximum value of $Re_{cr,unst} = 332$ for $\alpha = 22.6°$, and the corresponding values of $\delta_m^{cr,unst}$ become higher

(Fig. 8b). The following relationship for (α,$Re_{cr,unst}$) can be derived from the square best fit of numerical data :

$$Re_{cr,unst} = 0.200\alpha^2 - 0.038\alpha + Re_{cr,unst}^{\alpha=0^\circ}; \tag{6}$$

The mixing degree in the range for $Re_{cr,eng} \leq Re \leq Re_{cr,unst}$ follows a square root behavior for all the considered wall inclinations in the range $1.8 \leq \alpha \leq 22.6$, as shown in Fig. 9. This is in agreement with the previous findings in [21, 41–43], which found a similar behavior of the degree of mixing in arrow-shaped micro-mixers and in a mixing-separating device (H-geometry). We found that the an analogous relation holds for the wall-inclined T-shaped geometries investigated in the present paper in the engulfment regime, as we can write:

$$\delta_m - \delta_m^{cr,eng} = k_1 + k_2\sqrt{\frac{Re - Re_{cr,eng}}{Re_{cr,unst}}} \tag{7}$$

where the constant parameters, which were computed from the best fit of the numerical data, are $k_1 = 3.42$ and $k_2 = 57.25$.

5. Conclusions

The mixing process in a T-shaped mixer with inclined lateral walls has been analyzed through numerical simulations, in order to emulate the possible shapes of the device cross section obtained from the state-of-the-art production processes. Indeed, the present numerical study provides useful and practical indications on how flow regimes and mixing are affected by the lateral wall inclination that may stem either from the inaccuracy or the intrinsic features of the microfabrication technology. More specifically, we have investigated possible quantitative relationships between the values of the lateral-wall

inclination α, of the critical Reynolds numbers $Re_{cr,eng}$ and $Re_{cr,unst}$, when present, and of the mixing degree δ_m.

Considering a T-mixer fed with water, the same mixing performance as perfect square/rectangular cross-sections ([17]) is obtained for inclinations of the lateral walls below or equal to 3°. This inclination value can thus be considered as the maximum admissible error on the perpendicularity of the walls in the manufacturing process to keep the same mixing performance as the nominal configuration. Above this value, the presence of inclined walls is found to delay the onset of the engulfment regime at higher Reynolds numbers. The Reynolds number corresponding to the onset of the engulfment regime, and thus to a sudden increase in the mixing performance, monotonically increases with α and a quadratic relationship between $Re_{cr,eng}$ and α is found in the range $3 \leq \alpha \leq 22.6°$. An analogous quadratic function of α holds for $Re_{cr,unst}$, at which the unsteady periodic regime occurs. Moreover, in the engulfment regime the mixing degree performance follows a square-root behavior with Re typical of a supercritical instability (see e.g. [21]), and all the mixing-degree curves overlap if properly scaled with $(Re - Re_{cr,eng})/Re_{cr,unst}$ and $\delta_m - \delta_m^{cr,eng}$. For $\alpha \geq 23°$, the flow remains steady and does not enter the engulfment regime in the whole considered range of Re, i.e. $50 \leq Re \leq 350$, thus well above what happens for smaller lateral-wall inclination angles. Consequently, the degree of mixing remains significantly lower than those of smaller values of α.

However, at low Reynolds numbers, the mixing is moderately increased for $\alpha \geq 10°$, because the vortex regime presents a lower degree of symmetry with respect to the one of T-mixers with straight walls. One of the two

pairs of counter-rotating vortices overrides the other and moves towards the center of the mixing channel cross-section, while the other pair is confined to the bottom wall and weakens until it almost disappears. Nevertheless, single mirror symmetry is kept only, leading to a moderate mixing. Thus it can be concluded that when the wall inclination angle exceeds the identified critical value ($\alpha = 3$) a significant deterioration of the mixing performance occurs. Indeed, although mixing is slightly increased in the vortex regime, trapezoidal cross sections lead to a delay or to the complete disappearance of the engulfment regime.

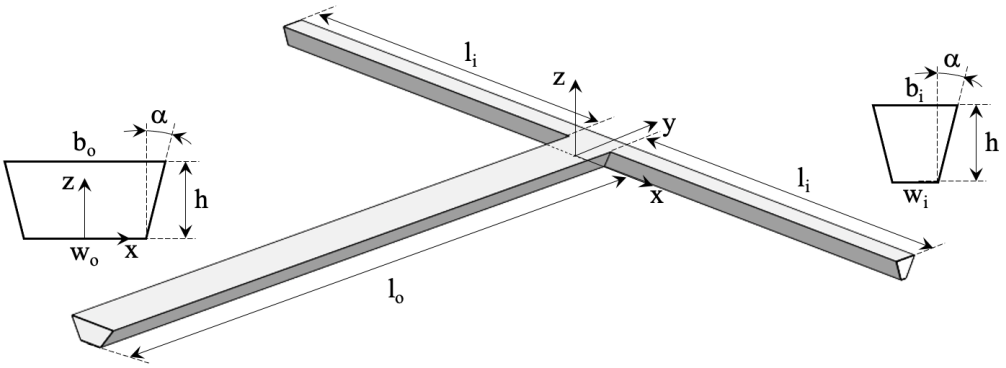

Figure 1: Sketch of the mixer geometry and reference system.

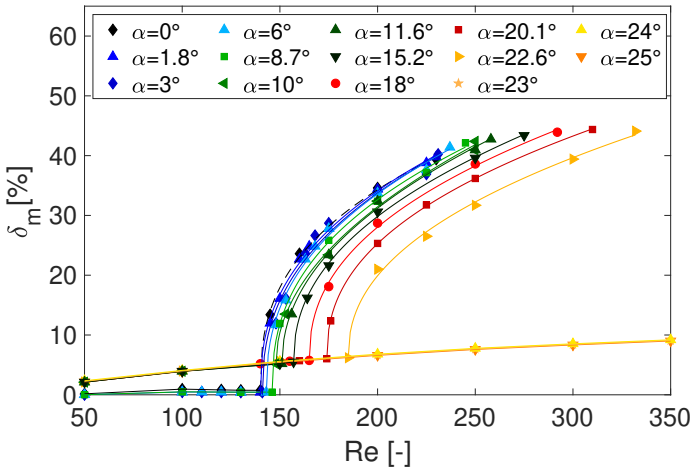

(a)

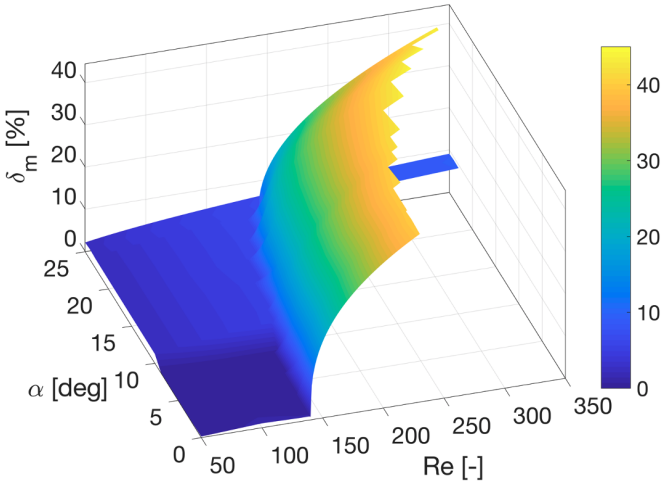

(b)

Figure 2: Mixing degree at the $Y = -8$ cross section: deterministic results (a) and response surface (b).

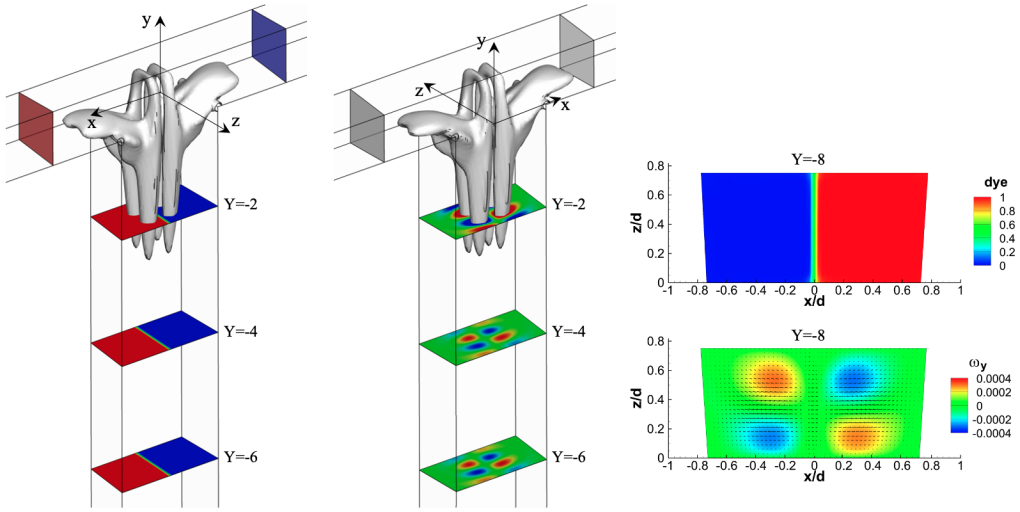
y
x
z
Y=-2
Y=-4
Y=-6
Y=-8
z/d
x/d
dye
1
0.8
0.6
0.4
0.2
0
ωy
0.0004
0.0002
0
-0.0002
-0.0004

(a)

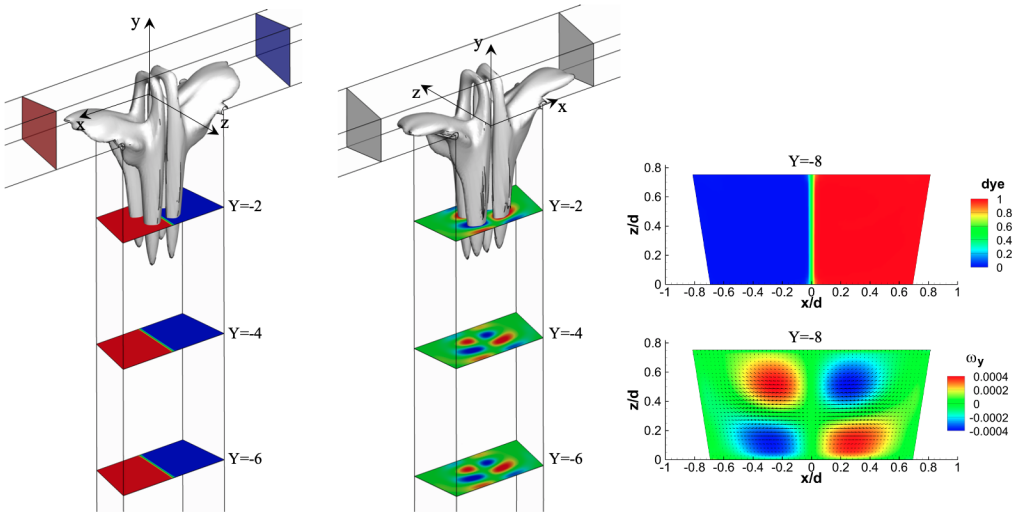
y
x
z
Y=-2
Y=-4
Y=-6
Y=-8
z/d
x/d
dye
1
0.8
0.6
0.4
0.2
0
ωy
0.0004
0.0002
0
-0.0002
-0.0004

(b)

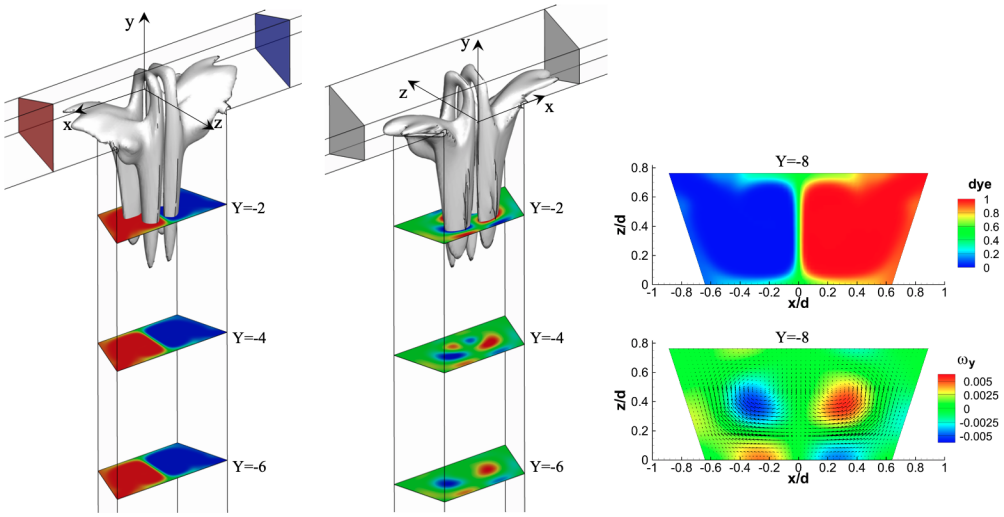

(c)

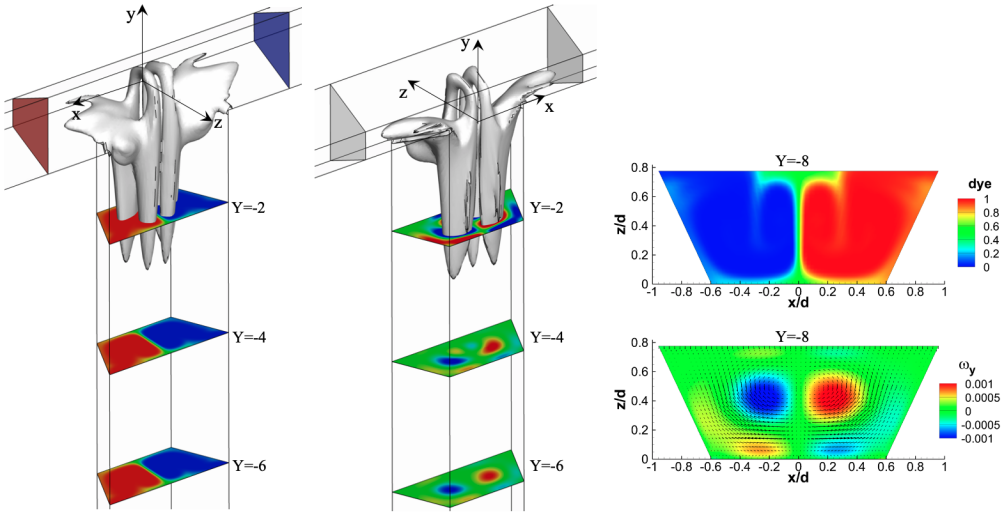

(d)

Figure 3: Isosurfaces of the vortex indicator λ_2 and dye-concentration field (left panel), isosurfaces of the vortex indicator λ_2 and $y-$vorticity field (central panel), dye-concentration field at the $Y = -8$ cross section (top-right panel) and in-plane velocity and $y-$vorticity at the $Y = -8$ cross section (bottom-right panel) at $Re = 100$. Considered cases: (a) $\alpha = 1.8°$, (b) $\alpha = 8.7°$, (c) $\alpha = 18°$, and (d) $\alpha = 25°$.

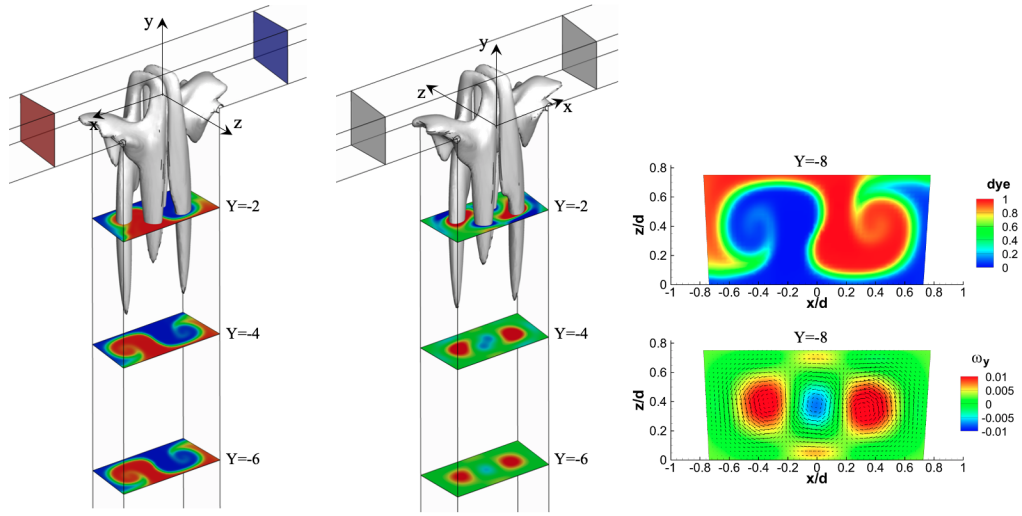
y
x
z
Y=-2
Y=-4
Y=-6
Y=-8
z/d
x/d
dye
1
0.8
0.6
0.4
0.2
0
ωy
0.01
0.005
0
-0.005
-0.01

(a)

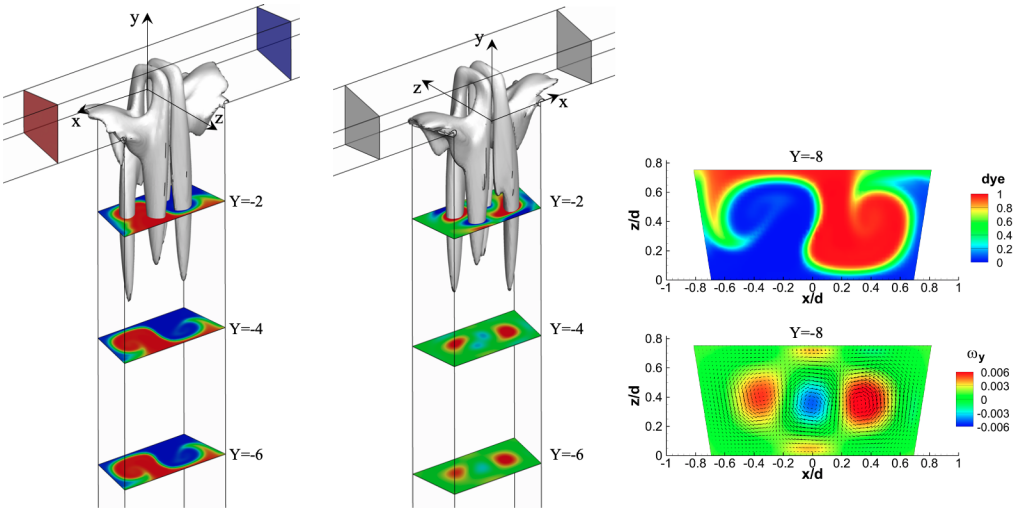
y
x
z
Y=-2
Y=-4
Y=-6
Y=-8
z/d
x/d
dye
1
0.8
0.6
0.4
0.2
0
ωy
0.006
0.003
0
-0.003
-0.006

(b)

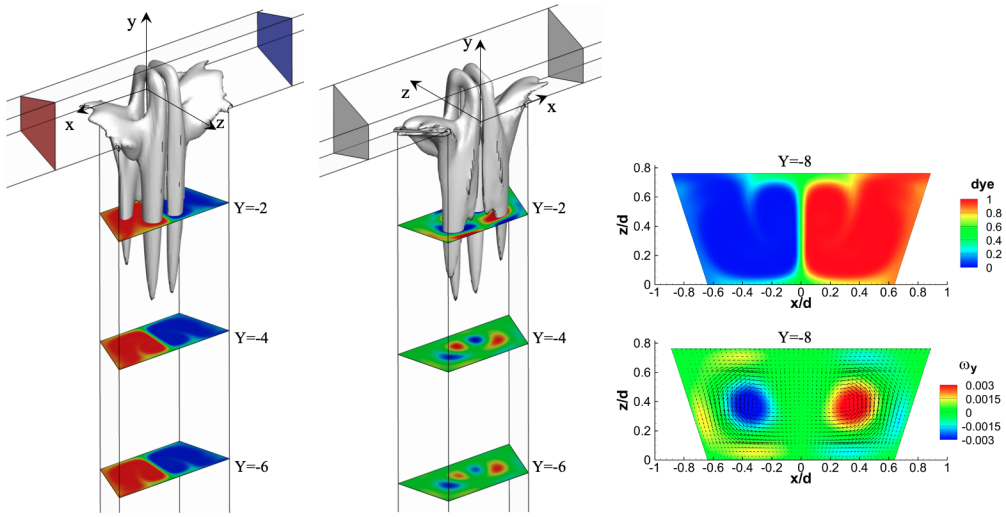

(c)

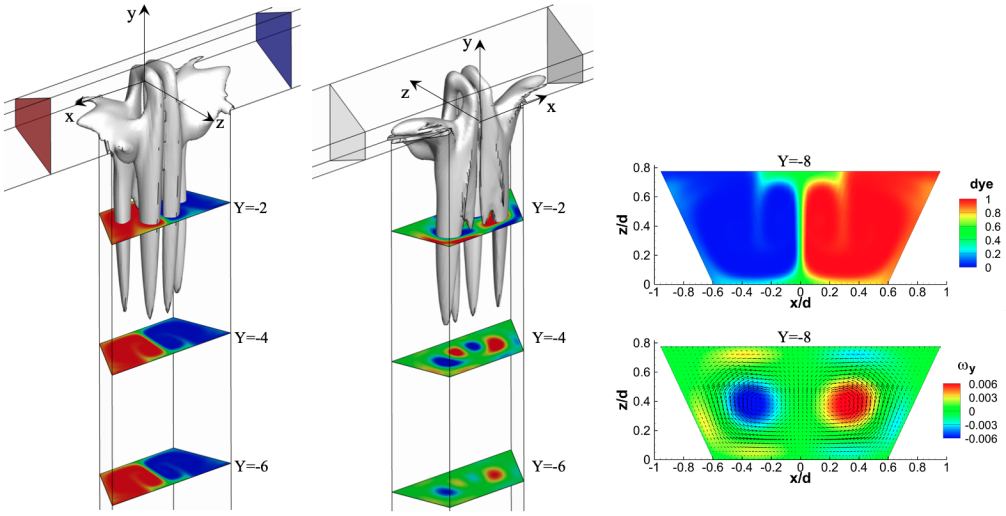

(d)

Figure 4: Isosurfaces of the vortex indicator λ_2 and dye-concentration field (left panel), isosurfaces of the vortex indicator λ_2 and $y-$vorticity field (central panel), dye-concentration field at the $Y = -8$ cross section (top-right panel) and in-plane velocity and $y-$vorticity at the $Y = -8$ cross section (bottom-right panel) at $Re = 150$. Considered cases: (a) $\alpha = 1.8°$, (b) $\alpha = 8.7°$, (c) $\alpha = 18°$, and (d) $\alpha = 25°$.

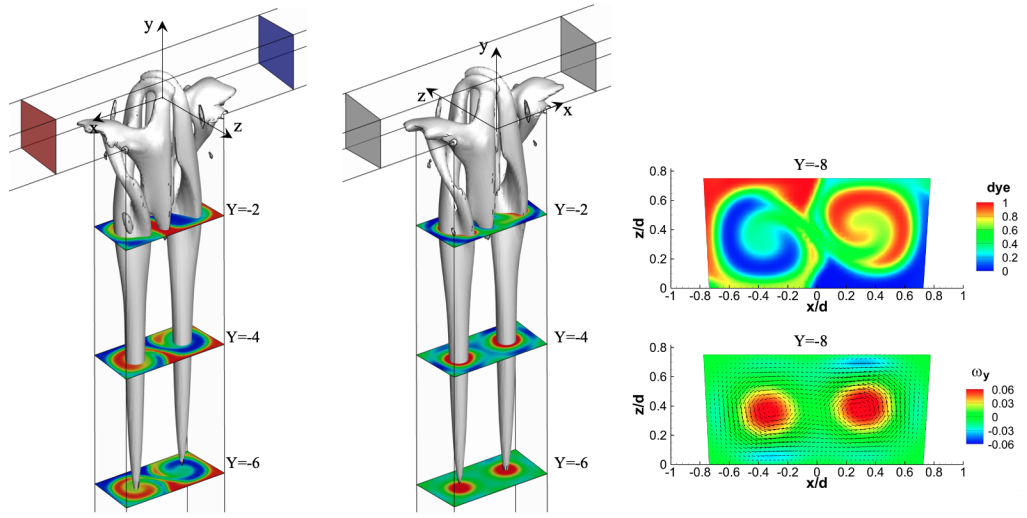
y
z
x
Y=-2
Y=-4
Y=-6
Y=-8
dye
1
0.8
0.6
0.4
0.2
0
z/d
x/d
ωy
0.06
0.03
0
-0.03
-0.06

(a)

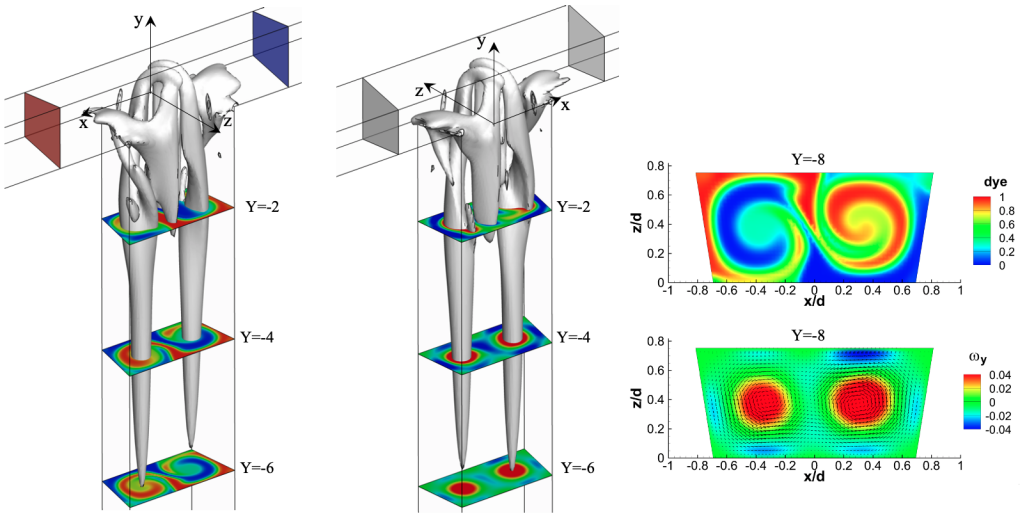
y
z
x
Y=-2
Y=-4
Y=-6
Y=-8
dye
1
0.8
0.6
0.4
0.2
0
z/d
x/d
ωy
0.04
0.02
0
-0.02
-0.04

(b)

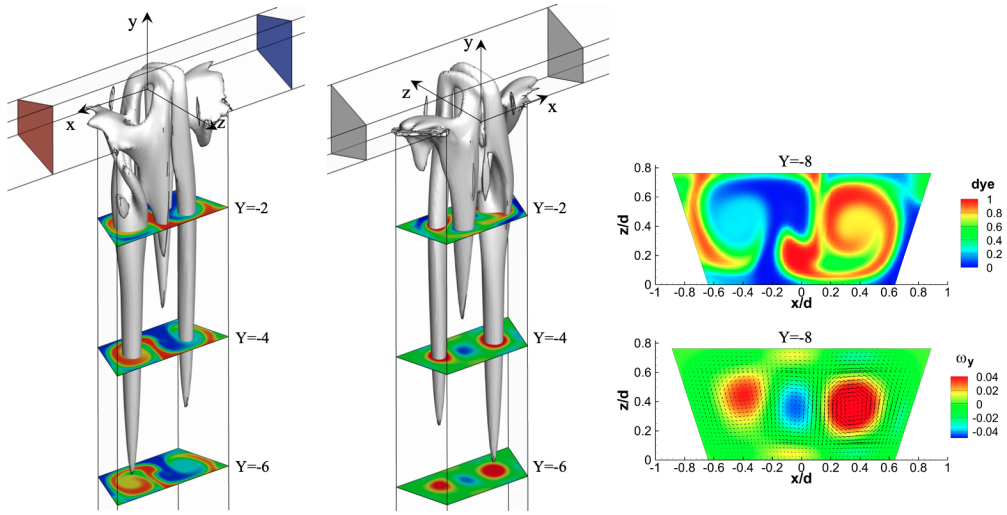

(c)

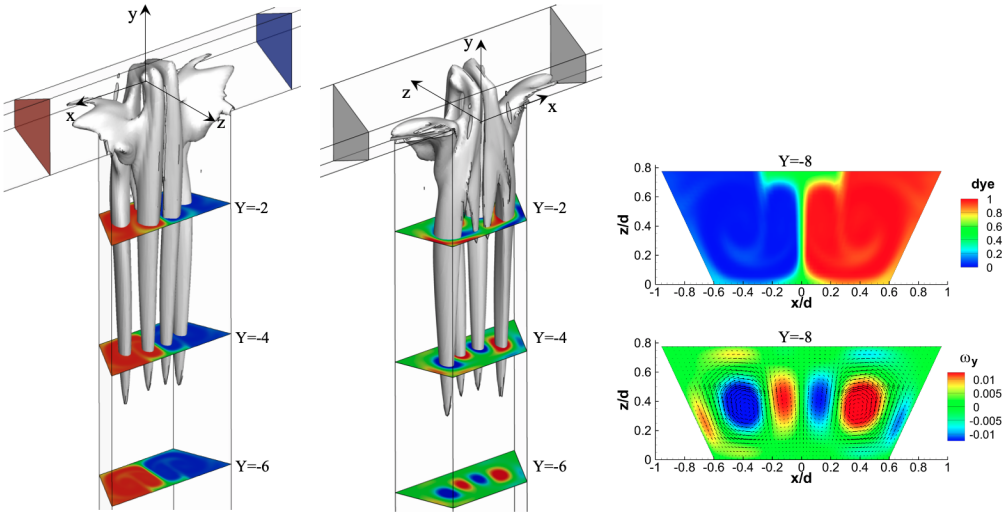

(d)

Figure 5: Isosurfaces of the vortex indicator λ_2 and dye-concentration field (left panel), isosurfaces of the vortex indicator λ_2 and $y-$vorticity field (central panel), dye-concentration field at the $Y = -8$ cross section (top-right panel) and in-plane velocity and $y-$vorticity at the $Y = -8$ cross section (bottom-right panel) at $Re = 200$. Considered cases: (a) $\alpha = 1.8°$, (b) $\alpha = 8.7°$, (c) $\alpha = 18°$, and (d) $\alpha = 25°$.

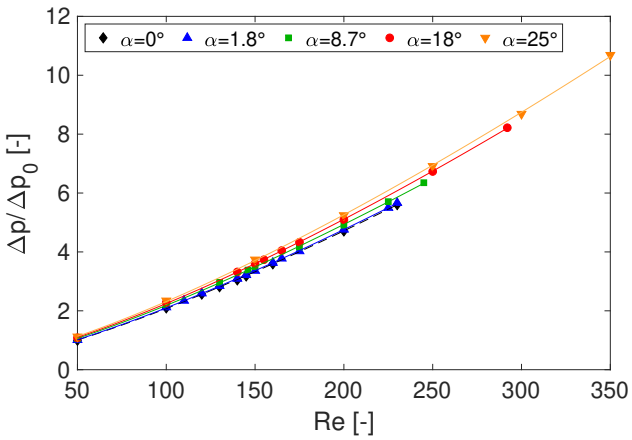

Figure 6: Pressure drops for the different wall inclination angles α.

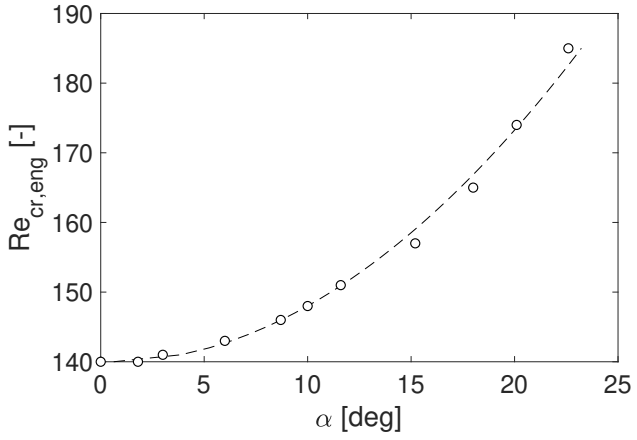

(a)

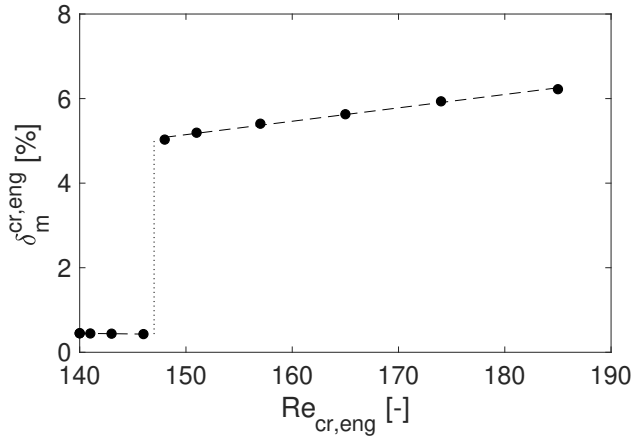

(b)

Figure 7: Onset of the engulfment regime: (a) critical Reynolds number, $Re_{cr,eng}$, as a function of the inclined-wall angle α and (b) corresponding degree of mixing as a function of the inclined-wall angle α.

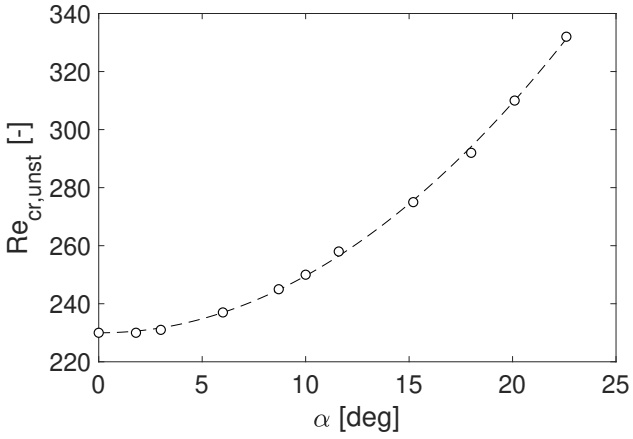

(a)

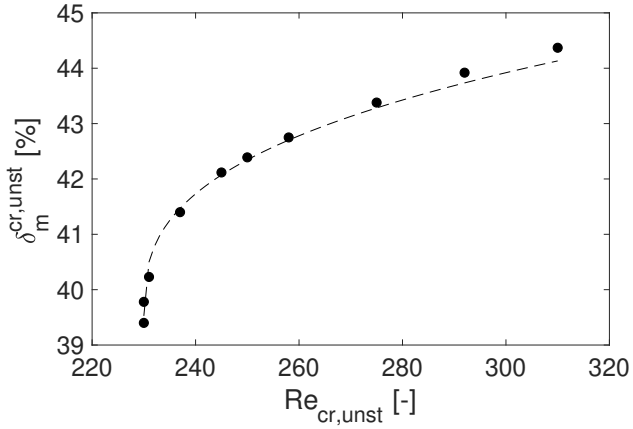

(b)

Figure 8: Onset of the unsteady regime: (a) critical Reynolds number, $Re_{cr,unst}$ as a function of the inclined-wall angle α and (b) corresponding degree of mixing as a function of the inclined-wall angle α.

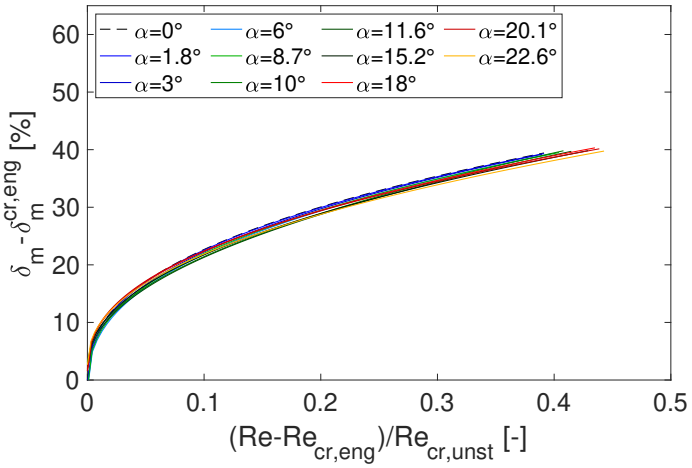

Figure 9: Rescaled mixing degree at the $Y = -8$ cross section.

References

[1] Aliaa I. Shallan and Craig Priest. Microfluidic process intensification for synthesis and formulation in the pharmaceutical industry. *Chemical Engineering and Processing - Process Intensification*, 142:107559, 2019.

[2] I. Rossetti and M. Compagnoni. Chemical reaction engineering, process design and scale-up issues at the frontier of synthesis: Flow chemistry. *Chemical Engineering Journal*, 296:56 – 70, 2016.

[3] P. Poechlauer, J. Colberg, E. Fisher, M. Jansen, M. D. Johnson, S. G. Koenig, M. Lawler, T. Laporte, J. Manley, B. Martin, and A. O'Kearney-McMullan. Pharmaceutical roundtable study demonstrates the value of continuous manufacturing in the design of greener processes. *Organic Process Research & Development*, 17(12):1472–1478, 2013.

[4] M. Riccomi, F. Alberini, E. Brunazzi, and D. Vigolo. Ghost particle velocimetry as an alternative to μpiv for micro/milli-fluidic devices. *Chemical Engineering Research and Design*, 133:183–194, 2018.

[5] R. Gani, J. Bałdyga, B. Biscans, E. Brunazzi, J.-C. Charpentier, E. Drioli, H. Feise, A. Furlong, K. M. Van Geem, J.-C. de Hemptinne, A. J. B. ten Kate, G. M. Kontogeorgis, F. Manenti, G. B. Marin, S. S. Mansouri, P. M. Piccione, A. Povoa, M. A. Rodrigo, B. Sarup, E. Sorensen, I. A. Udugama, and J. M. Woodley. A multi-layered view of chemical and biochemical engineering. *Chemical Engineering Research and Design*, 155:A133–A145, 2020.

[6] V. Kumar, M. Paraschivoiu, and K. D. P. Nigam. Single-phase fluid flow and mixing in microchannels. *Chemical Engineering Science*, 66(7):1329–1373, 2011.

[7] A. Mariotti, C. Galletti, E. Brunazzi, and M.V. Salvetti. Steady flow regimes and mixing performance in arrow-shaped micro-mixers. *Physical Review Fluids*, 4(3):034201, 2019.

[8] J.-W. Zhang, W.-F. Li, X.-L. Xu, H.-F. Liu, and F.-C. Wang. Experimental investigation of three-dimensional flow regimes in a cross-shaped reactor. *Physics of Fluids*, 31(3):034105, 2019.

[9] N. Ait Mouheb, D. Malsch, A. Montillet, C. Solliec, and T. Henkel. Numerical and experimental investigations of mixing in t-shaped and cross-shaped micromixers. *Chemical Engineering Science*, 68(1):278–289, 2012.

[10] A. S. Lobasov, A. V. Minakov, V. V. Kuznetsov, V. Ya Rudyak, and A. A. Shebeleva. Investigation of mixing efficiency and pressure drop in T-shaped micromixers. *Chemical Engineering and Processing - Process Intensification*, 134:105–114, 2018.

[11] S. Camarri, A. Mariotti, C. Galletti, E. Brunazzi, R. Mauri, and M.V. Salvetti. An Overview of Flow Features and Mixing in Micro T and Arrow Mixers. *Industrial and Engineering Chemistry Research*, 59(9):3669–3686, 2020.

[12] M. Bayareh, M. Nazemi Ashani, and A. Azam Usefian. Active and

passive micromixers: A comprehensive review. *Chemical Engineering and Processing - Process Intensification*, 147:107771, 2020.

[13] C. Chicchiero, L. Siconolfi, and S. Camarri. Investigation of the symmetry-breaking instability in a t-mixer with circular cross section. *Phys. Fluids*, 32(12):124106, 2020.

[14] N. Kockmann, C. Föll, and P. Woias. Flow regimes and mass transfer characteristics in static micro mixers. In *Proceedings of SPIE - The International Society for Optical Engineering*, volume 4982, pages 319–329, 2003.

[15] A. Soleymani, H. Yousefi, and I. Turunen. Dimensionless number for identification of flow patterns inside a T-micromixer. *Chemical Engineering Science*, 63(21):5291–5297, 2008.

[16] A. Mariotti, C. Galletti, R. Mauri, M.V. Salvetti, and E. Brunazzi. Steady and unsteady regimes in a T-shaped micro-mixer: Synergic experimental and numerical investigation. *Chemical Engineering Journal*, 341:414–431, 2018.

[17] A. Mariotti, C. Galletti, M.V. Salvetti, and E. Brunazzi. Unsteady Flow Regimes in a T-Shaped Micromixer: Mixing and Characteristic Frequencies. *Industrial and Engineering Chemistry Research*, 58(29):13340–13356, 2019.

[18] S. Dreher, N. Kockmann, and P. Woias. Characterization of laminar transient flow regimes and mixing in T-shaped micromixers. *Heat Transfer Engineering*, 30(1-2):91–100, 2009.

[19] S. Thomas, T. Ameel, and J. Guilkey. Mixing kinematics of moderate reynolds number flows in a T-channel. *Physics of Fluids*, 22(1):1–10, 2010.

[20] S. Thomas and T.A. Ameel. An experimental investigation of moderate reynolds number flow in a T-channel. *Experiments in Fluids*, 49(6):1231–1245, 2010.

[21] A. Mariotti, C. Galletti, E. Brunazzi, and M. V. Salvetti. Unsteady flow regimes in arrow-shaped micro-mixers with different tilting angles. *Physics of Fluids*, 33(1):012008, 2021.

[22] A. Fani, S. Camarri, and M. V. Salvetti. Investigation of the steady engulfment regime in a three-dimensional T-mixer. *Physics of Fluids*, 25(6):064102, 2013.

[23] C. Galletti, A. Mariotti, L. Siconolfi, R. Mauri, and E. Brunazzi. Numerical investigation of flow regimes in T-shaped micromixers: Benchmark between finite volume and spectral element methods. *Canadian Journal of Chemical Engineering*, 97(2):528–541, 2019.

[24] C. Galletti, E. Brunazzi, and R. Mauri. Unsteady mixing of binary liquid mixtures with composition-dependent viscosity. *Chemical Engineering Science*, 164:333–343, 2017.

[25] A. S. Lobasov and A. V. Minakov. Analyzing mixing quality in a T-shaped micromixer for different fluids properties through numerical simulation. *Chemical Engineering and Processing: Process Intensification*, 124(October 2017):11–23, 2018.

[26] T. Andreussi, C. Galletti, R. Mauri, S. Camarri, and M. V. Salvetti. Flow regimes in T-shaped micro-mixers. *Computers and Chemical Engineering*, 76:150–159, 2015.

[27] R. J. Poole, M. Alfateh, and A. P. Gauntlett. Bifurcation in a T-channel junction: Effects of aspect ratio and shear-thinning. *Chemical Engineering Science*, 104:839–848, 2013.

[28] A. Mariotti, M. Antognoli, C. Galletti, R. Mauri, M.V. Salvetti, and E. Brunazzi. The role of flow features and chemical kinetics on the reaction yield in a T-shaped micro-reactor. *Chemical Engineering Journal*, 396:125223, 2020.

[29] A. Mariotti, C. Galletti, R. Mauri, M.V. Salvetti, and E. Brunazzi. Effect of stratification on the mixing and reaction yield in a T-shaped micro-mixer. *Physical Review Fluids*, 6(2):024202, 2021.

[30] N. Kockmann, M. Engler, C. Föll, and P. Woias. Liquid mixing in static micro mixers with various cross sections. In *International Conference on Microchannels and Minichannels*, volume 1, pages 911–918, 2003.

[31] D.-K. Lee, J. Y. Kwon, and Y. H. Cho. Fabrication of microfluidic channels with various cross-sectional shapes using anisotropic etching of si and self-alignment. *Applied Physics A*, 125(5):291, 2019.

[32] Y. Peng, S. Jiang, L. Xia, X. Yin, B. Yu, and L. Qian. Direct ink writing combined with metal-assisted chemical etching of microchannels for the microfluidic system applications. *Sensors and Actuators A: Physical*, 315:112320, 2020.

[33] T. Wu, C. Ke, and Y. Wang. Fabrication of trapezoidal cross-sectional microchannels on pmma with a multi-pass translational method by co2 laser. *Optik*, 183:953–961, 2019.

[34] S. Zhang and Y. C. Shin. Effective methods for fabricating trapezoidal shape microchannel of arbitrary dimensions on polymethyl methacrylate (pmma) substrate by a co2 laser. *The International Journal of Advanced Manufacturing Technology*, 93(1):1079–1094, 2017.

[35] A. Mariotti, M. Lanzetta, G. Dini, A. Rossi, E. Brunazzi, R. Mauri, and C. Galletti. Influence of cross-sectional geometry on mixing in a T-shaped micro-junction. *Chemical Engineering Transactions*, 74:13340–13356, 2019.

[36] Al-Halhouli A, Al-Faqheri W, Alhamarneh B, Hecht L, and Dietzel A. Spiral microchannels with trapezoidal cross section fabricated by femtosecond laser ablation in glass for the inertial separation of microparticles. *Micromachines*, 9:171, 2018.

[37] J. Hussong, R. Lindken, M. Pourquie, and J. Westerweel. Numerical study on the flow physics of a T-shaped micro mixer. *in: M. Eller, X. Hu, J. Fröhlich, N. Adams (eds.) IUTAM Symposium on Advances in Micro- and Nano-fluidics*, 191, 2009.

[38] M. Bayareh. Artificial diffusion in the simulation of micromixers: A review. *Proceedings of the Institution of Mechanical Engineers, Part C: Journal of Mechanical Engineering Science*, 0(0):0954406220982028, 2020.

[39] C. Galletti, G. Arcolini, E. Brunazzi, and R. Mauri. Mixing of binary fluids with composition-dependent viscosity in a T-shaped micro-device. *Chemical Engineering Science*, 123:300–310, 2015.

[40] J. Jeong and F. Hussain. On the identification of a vortex. *Journal of Fluid Mechanics*, 285:69–94, 1995.

[41] S. J. Haward, R. J. Poole, M. A. Alves, P. J. Oliveira, N. Goldenfeld, and A. Q. Shen. Tricritical spiral vortex instability in cross-slot flow. *Phys. Rev. E*, 93:031101(R), 1–5, 2016.

[42] W. M. Abed, A. F. Domingues, R. J. Poole, and D. J. C. Dennis. Heat transfer enhancement in a cross-slot micro-geometry. *Int. J. Therm. Sci.*, 121:249–265, 2017.

[43] A. F. Domingues, R. J. Poole, and D. J. C. Dennis. Inertial instabilities in a microfluidic mixing-separating device. *Phys. Fluids*, 31:074101, 1–16, 2019.